Journal of Renewable Materials

Tech Science Press

DOI: 10.32604/jrm.2021.012271

ARTICLE

A Promising Wound Dressing from Regenerated Silk Fibroin Sponge with Sustain-ed Release of Silver Nanoparticles

Yang Li[#], Xiaoying Zha[#], Xingliang Xiong, Yan Zhang, Ying Feng, Haojiang Xie, Linqing Zhang and Qifeng Jiang[*]

Department of Medical Information, Chongqing Medical University, Chongqing, 400016, China

[#]The authors contribute equally

[*]Corresponding Author: Qifeng Jiang. Email: jiangqf@cqmu.edu.cn

Received: 23 June 2020 Accepted: 15 September 2020

ABSTRACT

A silk fibroin (SF) spongy wound dressing incorporated with silver nanoparticles (Ag-NPs) was developed for biomedical applications. Ag-NPs were efficiently synthesized *in situ* via ultra violet (UV) with $AgNO_3$ as precursor and silk fibroin as reducing and protecting agent, respectively. After lyophilization, the formed silk fibroin spongy wound dressing (SFWD) exhibited polyporous morphology and inner lamellae structures, with uniform dispersion of Ag-NPs. The porous structure provided SFWD with the ability to absorb tissue exudatealmost 6 times of its own weight, which could guarantee the sustained release of Ag-NPs. By methanol treatment, SFWD showed much improved mechanical properties and more stable to protease XIV. The cyto-compatibility of SFWD was supported by normal adherence and proliferation of NIH3T3 fibroblasts in sponges extracting culture medium. More important, the SFWD showed significant growth inhibition in both plate culture assays and bacterial suspension assays, with Gram-positive (*Staphylococcus aureus*) and Gram-negative (*Pseudomonas aeruginosa* and *Escherichia coli*). In a cutaneous excisional mouse model, the average healing rates of SFWD was significantly higher than control and commercial bandages. The hematoxylin-eosin (HE) staining results of the wound section also showed that SFWD could recruit more cells and promote tissue formation on the wound edges.

KEYWORDS

Silk fibroin; sponge; antibacterial activity; wound dressing

1 Introduction

Skin is a critical barrier in human body to protect organs against external changes and microbial infection. However, trauma and burns often cause tissue necrosis and destroy the defense function of skin [1]. From the moment skin wound is created, many complications might develop, causing microbial invasion, hindering regeneration of epidermal tissue, delaying wound healing, and promoting scar formation [2]. The efficient healing process is often accompanied by use of wound dressings, which serve as a shield against external factors like dust and bacteria. An ideal wound dressing should maintain a moist environment in the wound and permit the exchange of water and gas, promote epithelialization by releasing biological agents to the wounds [3]. Considering these unique properties, naturally-derived silk fibroin (SF) has been emerged into the development of wound dressings [4].

SF is a natural protein which mainly derives from the *Bombyx mori* silk worm cocoons. Due to its superior cyto-compatibility, bio-degradation, and permeability, SF has demonstrated excellent properties for wound dressing. SF-based dressing also showed exceptional characteristics as carrier to deliver drugs and bioactive nanoparticles to wound sites for promotion of healing [5]. With different preparation process, the SF can be cast into various forms, such as films, gels, hydrogels and sponges. In particular, because of the porous structure, sponges have promising capacity for encapsulation of drugs and bioactive nanoparticles, which could inhibit bacterial growth and prevent infection [6]. Besides, the release behavior of these compounds to the wound sites from sponges is tunable, based on manipulation of control points during the process of preparing the sponges, including the molecular weight and beta-sheet formation [7]. Therefore, in this work, the silk sponges were fabricated through lyophilization, and utilized as a wound dressing substrate, the mechanical and degradation properties of the sponges were tuned via controlling concentration of silk fibroin and beta-sheet content [8,9].

To date, many metal nanoparticles were utilized in medical, such as gold, silver and copper, owing to their antibacterial properties [10,11]. Among these metal nanoparticles, silver is preferred because of low cost, broad-spectrum antibacterial properties and easy fabrication [11]. The previous studies have illustrated that silver particles would not inhibit epidermal cell proliferation, meanwhile possessing antibacterial properties against *Staphylococcus aureus*, *Pseudomonas aeruginosa*, and Esche-richia coli. Actually, silver can inhibit many microorganisms, including Gram-negative bacteria, Gram-positive bacteria, fungi, and viruses, via interfering inner biomacromolecule [12,13].

The objective of the present study was to fabricate a promising silver-containing wound dressing, which could prevent wound infection and promote wound healing, with easy preparation and low price. Ag-NPs were fabricated *in situ* by UV irradiation with silk fibroin serving as stabilizer, dispersant and protector, which could ensure the uniform formation of Ag-NPs in sponges [14,15]. The characterization of sponge was probed with Scanning Electron Microscopy (SEM) and Fourier Transform Infrared Spectroscopy (FTIR), and the formation of Ag-NPs was confirmed with Energy Dispersive Spectrometer (EDS). The viability of NIH3T3 fibroblasts was used to Characterize cytocomptibility. The antibacterial activity of sponge was confirmed with Gram-positive (*Staphylococcus aureus*) and Gram-negative (*Pseudomonas aeruginosa* and *Escherichia coli*). Besides, a cutaneous excisional mouse model was used to dynamically present the healing effect of sponge in full-thickness skin defect.

2 Experiment Section

2.1 Basic Materials

Lithium bromide(Sinoreagent); Dialysis Membranes (Solarbio); silver nitrate (Sinoreagent); Simulated body fluid (Sigma-Aldrich); protease XIV solution (Sigma-Aldrich); *Staphylococcus aureus*, *Pseudomonas aeruginosa* and *Escherichia coli* (Shanghai S & S Biotechnology Co., Ltd., China); Mueller-Hinton Broth (MHB) Agar (Thermo Scientific); DMEM culture medium (Gibico); CCK-8 kit (Maclin, China)

2.2 Preparation of Silk Fibroin Solution

SF solution was prepared from *Bombyx mori* silkworm cocoons (SOUTHWEST UNIVERSITY, Chongqing, China) as described previously [6,16]. Briefly, silkworm cocoon was boiled in a 0.02 M sodium carbonate solution for 30 min, rinsed and dried in draught cupboard overnight. Dried fibroin was dissolved in lithium bromide solution (9.3 M) at 60°C for 4 h. The obtained solution was continually dialyzed for 2 days with Dialysis Membranes (molecular weight cut-off = 3500 DA) to remove the lithium bromide. The dialyzed solution was centrifuged with 9000 rpm to remove insoluble substance and the final concentration of fibroin was 6%–7% wt/v, then stored at 4°C [17].

2.3 Fabrication of SWFD

For a typical fabrication procedure, certain amount of silver nitrate ($AgNO_3$) powder was added into 6 wt% SF solution and blended in beaker to form a transparent SF-$AgNO_3$ mixture solution and the final concentration of $AgNO_3$ was 0.02%, 0.04%, 0.08% (wt/v), respectively. Then the SF-$AgNO_3$ mixture solution was placed under ultraviolet lamp, irradiated at wavelength of 365 nm for 6 h. Microplate Reader (Multiskan, Thermo Fisher scientific, Co., China) was then used to conform the formation and dispersity of Ag-NPs. The irradiated solution was placed in 24-orifice plate, followed by pre-freezing at −20°C for 1 h and −80°C overnight [18]. The pre-freezing sponges were then lyophilized for 36 h and immersed in 90% (v/v) methanol with 30 mins to induce beta-sheet formation. After rinsed with ultra-pure water, the SF/Ag-NPs sponges were dried in 60°C [18,19].

2.4 Water Absorption

Simulated body fluid (SBF) was utilized to measure water absorption capacity of the SWFD. Briefly, SWFD were prepared according to the above method, recording the mass as m. Lyophilized sponges were immersed in SBF for 30 min, recording the mass as M [13]. The calculation formula of water absorption is as follows:

$$\text{Wt\%} = (M - m)/m \times 100 \quad (1)$$

Wt% is water absorption; m is lyophilized sponge mass; and M is hydrated sponge mass.

2.5 Morphology Characterization of SWFD

SWFD morphology was investigated by scanning electron microscopy (ZEIS-S sigma 300), with accelerating voltage of 10 kV. The sponge fraction was mounted on sample abutment, cross-section oriented top, and then the porous structures of sponges prepared from different concentration were probed. Energy Dispersive X-ray Spectroscopy (EDS) analysis were carried out to determine the existence of silver in sponges. In order to observe the conformational changes of SFWD via methanol post-treatments, Fourier Transform Infrared Spectroscopy analysis was utilized to determine the beta-sheet content of it. The dried SFWD were ground into powder with potassium bromide (KBr), and pressed into flake for FTIR measurement using NICOLET iS50 FT-IR spectrometer. For each measurement, 64 scans were recorded with resolution 0.5 cm^{-1}, and the wave numbers ranged from 600 to 4000 cm^{-1} [20–22].

2.6 Characterization of Mechanical Properties

In order to investigate the tensile fracture strength of SFWD with various concentration, 3% and 6% wt/v SFWD were cast into strips with uniform diameter of 25 mm × 6 mm × 3 mm. Microcomputer Controlled Electronic Universal Testing Machine (Shanghai Yihuan Instrument Technology Co., Ltd., China) was utilized to measure the tensile strength of SFWD prepared from different concentration [23,24].

2.7 In Vitro Degradation

In vitro degradation of SFWD was analyzed by protease XIV solution (Sigma-Aldrich, St. Louis, MO). SFWD were dried at 60°C oven then cut into cylindrical (diameter = 20 mm, height = 2 mm) and weighed. Then each sample was placed in 2 mL of 1 U/mL Protease XIV solution incubated at 37°C for 5–9 d. After incubation, the samples were dried at 60°C and weighed again [16,17,25]. The weight loss was calculated according to the following equation:

$$\text{WR \%} = WR/Wi \times 100 \quad (2)$$

The WR is weight remaining and the Wi is the initial weight.

2.8 Antibacterial Assays

The antibacterial activity of SFWD was tested against *Staphylococcus aureus*, *Pseudomonas aeruginosa* and *Escherichia coli* (Shanghai S & S Biotechnology Co., Ltd., China). Mueller-Hinton Broth (MHB) Agar was used as culture medium. For the plates culture assays, the SFWD ($AgNO_3$ concentration 0.02, 0.04, 0.08% wt/v) and negative control group (pure SF sponges) were cut into discs with 8mm diameter and placed on each *S. aureus*, *P. aeruginosa* and *E. Coli* MHB Agar plates, and then incubated at 37°C overnight. The inhibition zones diameter was measured after 24 h incubation [26,27]. For the bacterial suspension assays, 400 μL bacterial suspension was added into flasks with 20 mL MHB medium and the SFWD ($AgNO_3$ concentration 0.02, 0.04, 0.08% wt/v), negative control group (pure SF sponges) and blank group, and incubated at 37°C for 24 h. Optical density (OD) measurement at 600 nm was scheduled with 100 μL of bacterial solution from each flaskat time point of 0, 2, 4, 6, 8, 10, 12 and 24 h, respectively [13,28].

2.9 Cytocompatibility of SFWD

The SFWD ($AgNO_3$ concentration 0.08% wt/v) and control were cut into cylindrical (diameter = 20 mm, height = 10 mm) and all samples were sterilized with ethanol and UV radiation for 1 h [29–31] and then incubated in 50 ml extraction medium (DMEM, supplemented by 10% fetal bovine serum, 1% L-glutamine and 1% antibiotics) for 3 days at 37°C in 5% CO_2. NIH3T3 fibroblasts (Solarbio, Beijing, China), were cultured in 96-well plates with 6000 cells per well in fresh DMEM, supplemented by 10% fetal bovine serum, 1% L-glutamine and 1% antibiotics and extraction DMEM respectively, at 37°C in 5% CO_2 for 1 day till nearly full attachment [1]. The cell viability was determined by Cell Counting Kit-8 (CCK-8; Solarbio, Beijing, China), and the absorbance was detected by Microplate Reader (Multiskan, Thermo Fisher scientific Co., China) at 450 nm [26,32].

2.10 Wound Healing

Sixteen healthy 8-week-old male Kunming mice (approved by the Ethics Committee of Chongqing Medical University) were procured from animal center of Chongqing Medical University, Chongqing, China with weight between 34 g and 39 g. These mice were maintained and acclimated for 1 week in an animal facility under standard laboratory conditions for this study, with water and standard provided adlibitum. Their dorsum was cut by sterile surgical scissors, with the uniform size wounds, about 6 mm in diameter. The treated mice were randomly divided into four groups: SFWD ($AgNO_3$ concentration 0.08% wt/v), pure SF sponge, Bandage and Blank group. On the 1st, 3rd, 5th, and 9th day, the average size of wounds in each mouse was measured and recorded. The percentage of residual wound size to original wound size was used to represent the healing rate, and the ratio was inversely proportional to the healing rate [21,33]. At end of each time point, the mice were sacrificed and the specimens from the whole wound site were harvested for Hematoxylin and Eosin (HE) staining [34].

3 Results and Discussion

3.1 Characterization of Ag-NPs Formation in Silkfibroin Solution

To determine the Ag-NPs formation in the composite silk solution, microplate reader (Multiskan, Thermo Fisher scientific, Co., China) was used to probe the absorption curve of Ag-NPs. As shown in Fig. 1, significant peaks around 400 nm could be observed in silk solution with different concentrations of silver nitrate, except control group, which proved that Ag-NPs had been successfully produced [14,15]. Moreover, peak value around 400 nm increased with the increase of silver nitrate concentrations, indicating the promotion of Ag-NPs content. In this study, Ag-NPs were fabricated *in situ* by UV irradiation, and silk fibroin might serve as stabilizer, dispersant and protector, which could ensure the uniform formation of Ag-NPs in sponges. The beauty of this preparation was the combination of sponge fabrication and Ag-NPs formation at the same time, with high-efficiency and low-cost.

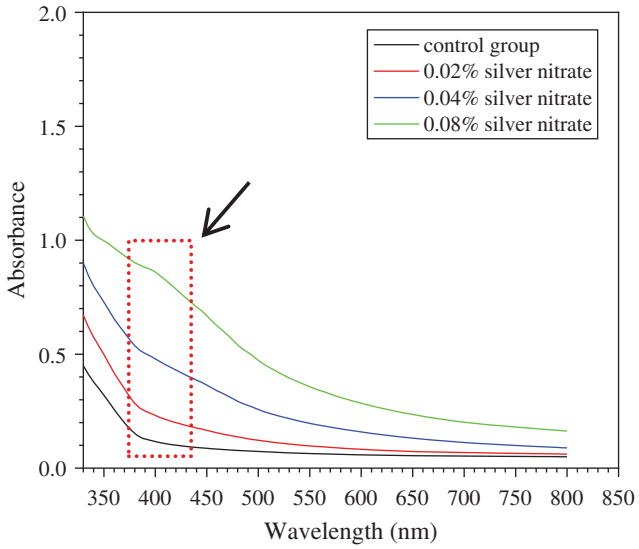

Figure 1: Characterization of Ag-NPs-containing SF solution: The absorption curve of silk solution containing various concentrations of silver nitrate. Arrow presents the adsorption peak

3.2 Shape and Water Absorption of SFWD

SFWD were prepared from silk solution with 1, 3, and 6% wt/v concentration, respectively. As shown in Fig. 2a, the low silk concentration (1% wt/v) of sponges didn't have stable shape and were easy to collapse, compared with higher fibroin concentration. So, all sponges were prepared from 3 and 6% wt/v concentration in follow-up study. Water absorption is an important feature for wound dressing, which is closely related to drug sustained release and tissue exudate absorption [3]. The ideal wound dressing can quickly absorb tissue exudate to prevent wound infection, and at the same time, it will continuously release the loaded drugs through structural expansion to promote wound healing. In present study, SBF was used to determine the water absorption of SFWD in different conditions. As shown in Fig. 2b, all groups possessed superior water absorption capacity which was approximately 600%. Besides, there was no significant difference among the groups. The results showed that SFWD can effectively absorb the tissue exudate from the wound, which might suggest that once SFWD is placed on the wound site, it would keep the wound in relatively dry condition, reduce the possibility of inflammation and promote wound healing.

3.3 Porous Morphology of SWFD

The porous morphology of SWFD was determined with SEM analysis. SFWD were cast from 3% and 6% (wt/v) concentration and the scanning electron microscopic images were Figs. 3a–3c and Figs. 3d–3f, respectively. Both sponges exhibited a network of thin, sheet-like lamellae with inner porosity. Besides, SFWD cast from high silk concentration solution had thicker lamellae and more difficultly to collapse than low concentration silk solution which possessed lager pores. The porous structure could provide large surface area which ensured SFWD had improved loading capacity of Ag nanoparticles. In the meantime, the porous structure endowed SFWD with stronger water absorption capacity, which might explain the promoted water absorption of SFWD. The elemental silver signal in EDS confirmed the integration of Ag nanoparticles in fibroin sponges (Fig. 3g). Strong signals of C, N and O were also detected mainly from the backbone of silk. Considering the weak absorption peak around 400 nm in EDS, SEM was used to directly visualize the formation of Ag nanoparticles in SFWD. As shown in Figs. 3h and 3i, random distribution of Ag nanoparticles could be found inside SFWD.

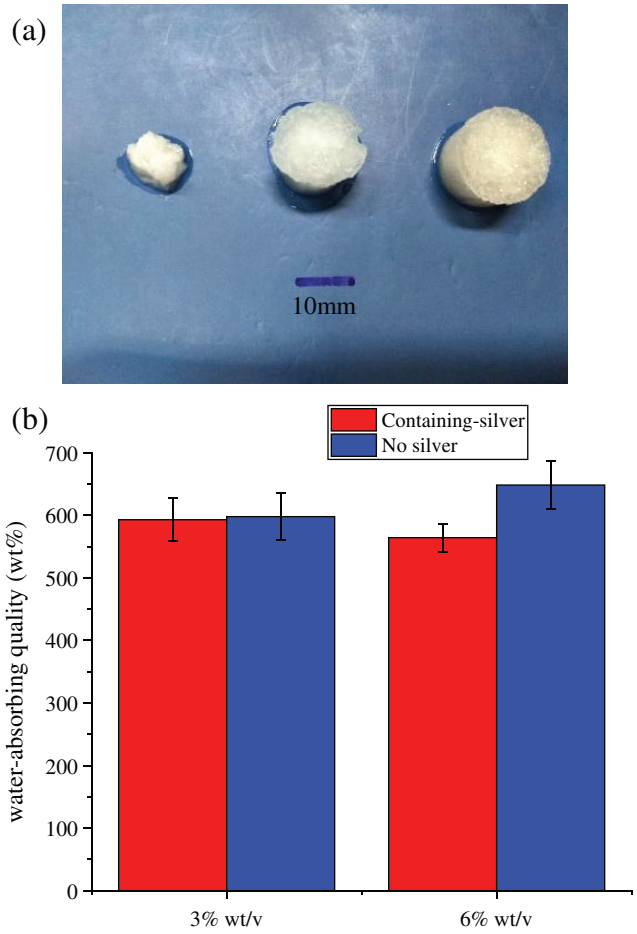

Figure 2: Shape and water absorption of SFWD. (a) Hydrated SFWD prepared from silk solution with 1, 3 and 6% (wt/v) concentration (left to right); (b) Absorption capacity of SFWD (n = 4).

3.4 The Structural Characteristics of SFWD after Methanol Treatment

The changes of secondary structure in SFWD samples after methanol treatment was determined by Fourier Transform Infrared spectroscopy (FTIR). The infrared spectra region between 1580 to 1720 cm^{-1} was selected for further analyze. Figs. 4a and 4b showed the peak absorption bands were assigned as follows: in Fig. 4a, 1610–1630 cm^{-1} and 1698–1708 cm^{-1} as beta-sheet structure; 1630–1644 cm^{-1} as random-coil structure; 1644–1663 cm^{-1} as alpha-helical bands; 1663–1698 cm^{-1} as beta turns; in Fig. 4b, 1610–1624 cm^{-1} and 1693–1704 cm^{-1} as beta-sheet structure; 1646–1674 cm^{-1} as random-coil structure and alpha-helical bands; 1674–1693 cm^{-1} as beta turns [2,16]. The content of beta-sheet significantly increased from 17.32% to 39.41%, after methanol treatment, which proved the transition of fibroin structure from random-coil to beta-sheet via methanol treatment.

3.5 Effect of SF Concentration and Beta-Sheet Formation on Mechanical Properties of SWFD

Tunable mechanical properties are critical for wound dressing, different site of wound may require the wound dressing with specific strength [20]. Ultimate Tensile Strength (UTS) was used to assess the mechanical strength of SWFD. As shown in Fig. 5, the UTS of SWFD significantly increased with increase of fibroin concentration. UTS of the sponges casted from 3% and 6% SF solution were 38.33 ± 2.89 kPa and 140.00 ± 5.00 kPa, respectively. Besides, methanol treatment improved the strength of

SFWD in both 3% and 6% concentration. After methanol treatment, UTS of SFWD prepared from 3% and 6% silk solution were 73.33 ± 5.77 kPa and 180.00 ± 18.03 kPa, respectively. With this feature, tunable mechanical properties of SFWD were matched to diverse wounds types, via altering the parameters of fabrication, SFWD could obtain different strength, which could be customized for different site of wound healing [20,35].

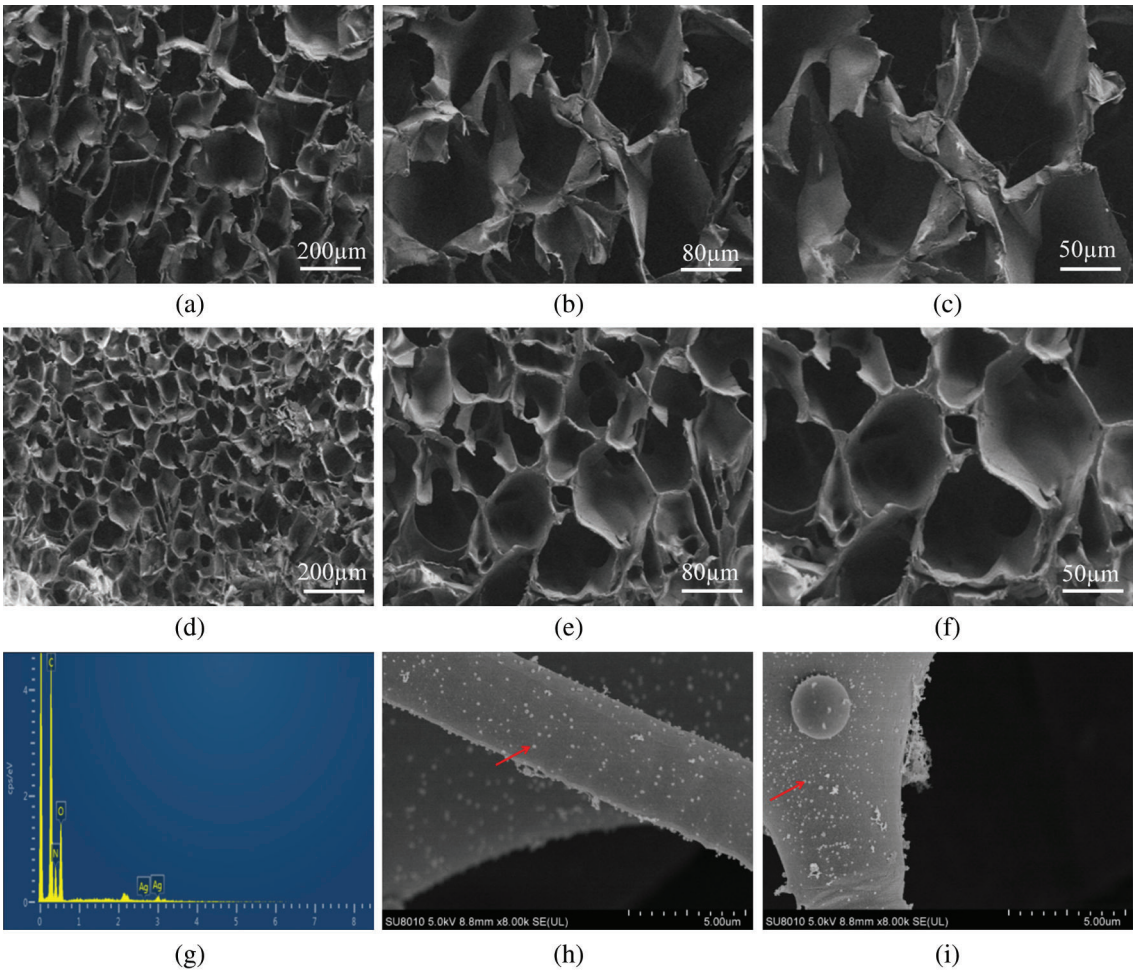

Figure 3: The SEM morphology of cross section from SFWD. (a–c) sponges cast from 3% (wt/v) silk solution with 80, 200 and 300 magnification, respectively; (d–f) sponges cast from 6% (wt/v) silk solution with 80, 200 and 300 magnification, respectively; (g) EDS of Ag-NPs-containing scaffolds; (h, i) The formation of Ag-NPs in SFWD (red arrows)

3.6 In Vitro Degradation of SWFD

The stability to protease is an important factor in the drug sustained release from wound dressings. High degradation rate might lead to burst release of drug which might attenuate the wound healing process [25]. To study the effect of beta-sheet contents and protein concentration on degradation properties of SFWD, Protease XIV was utilized to determine silk degradation *in vitro*. Protease XIV is a cocktail of bacterial protease which has been frequently utilized in silk degradation mechanism. Silk degradation was determined by the ratio between remaining and initial mass, after immersing in Protease XIV at 37°C for 1, 2, 3, 5, 7 and 9 days, Respectively. Fig. 6 showed that SFWD prepared with higher concentration (6%)

were much more stable in Protease XIV than the lower concentration (3%). Moreover, the degradation rate of methanol treated SFWD was much lower than untreated, in both 3% and 6% concentration. These results are parallel with previous studies that silk fibroin degradation is related to content of beta-sheet crystallinity, which could be induced by methanol treatment. In present study, the degradation rate of SFWD could easily tuned by SF concentration and methanol treatment. With different degradation rate, SFWD would keep stable to Protease XIV in different time course, which might control duration of the sustained release of Ag nanoparticles. Besides, this biodegradability could guarantee SFWD might be used not only on the body surface, but also inside of body [25,36].

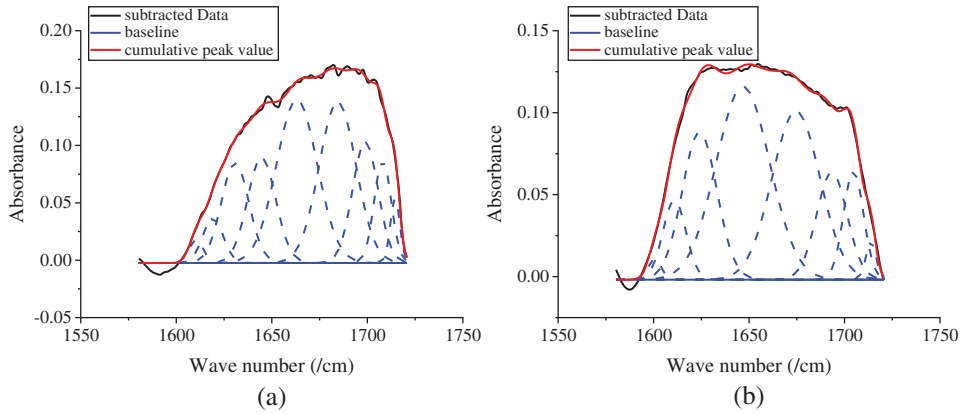

Figure 4: Peak absorbance figure of the samples in analysis software. (a) before-treatment by methanol; (b) after-treatment by methanol

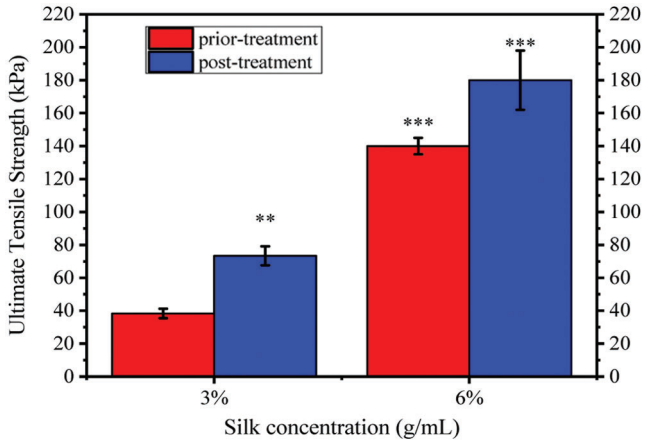

Figure 5: Effects of fibroin concentration on shape and mechanical strength of SFWD: Ultimate Tensile Strength of SFWD with 3 and 6% concentration before and after methanol treatment. (*: $p < 0.05$, **: $p < 0.01$, ***: $p < 0.001$, n = 5)

3.7 Antibacterial Properties of SWFD

The antibacterial activity of SWFD against *Staphylococcus aureus*, *Pseudomonas aeruginosa* and *Escherichia coli* was shown in Fig. 7. For the bacterial suspension assays, the antibacterial properties of SWFD were evaluated with OD value at different timepoint with different silver nitrate concentration. The OD value was detected every two hours (Figs. 7a, 7c, and 7e), and the ultimate OD value was

measured after 24 h (Figs. 7b, 7d, and 7f). As shown in Figs. 7a, 7c, and 7e, all SFWD with different concentration of Ag-NPs significantly inhibited bacterial growth. Moreover, as shown in Figs. 7b, 7d, and 7f, among three different concentration of silver nitrate, 0.08% groups exhibited the strongest antibacterial activity. The antibacterial activity of SFWD in the plates culture assays was shown in Figs. 7g, 7h, and 7i. The antibacterial activity of SFWD with different concentrations of silver nitrate was presented by inhibition zones in *Escherichia coli, Pseudomonas aeruginosa*, and *Staphylococcus aureus*, respectively. The inhibition zones showed that with higher concentrations of silver nitrate, antibacterial properties of SFWD increased.

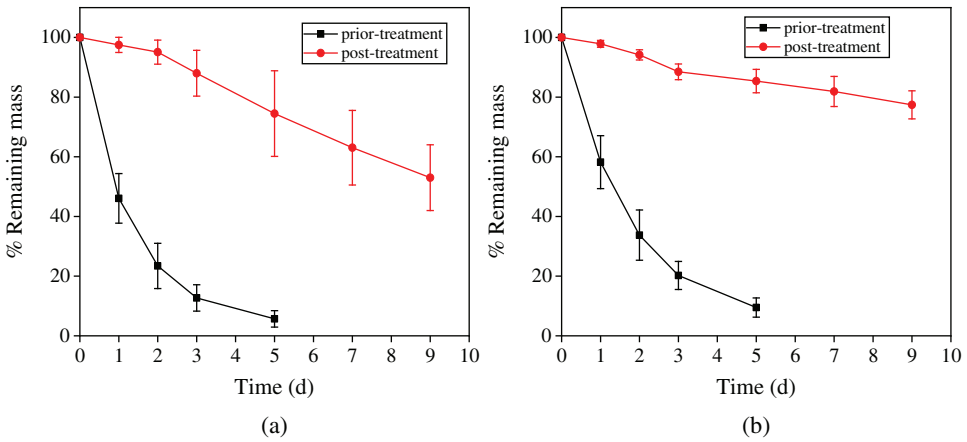

Figure 6: Effect of concentration and beta-sheet content on degradation of SFWD *in vitro* enzymatic. (a) Degradation of 3% wt/v scaffolds. (b) Degradation of 6% wt/v scaffolds. (n = 4)

3.8 Cyto-Compatibility of SWFD

Cyto-compatibility is a key parameter for clinical use of all wound dressing. The cyto-compatibility of SWFD was determined with NIH3T3 fibroblasts. Cell Count Kit-8 (CCK-8) reagent was used to detect cell viability. Figs. 8a–8e showed that SWFD group cells presented similar morphology with control group. Mostly of the cells adhered and spreaded normally with SWFD extraction medium. Besides, as shown in Fig. 8f, there was no significant difference of cell viability among SWFD group and control group, which indicated SWFD possessed superior cyto-compalibility.

3.9 Wound Healing Analysis

SWFD and commercial bandages were applied on the excisional wounds of the dorsum sides of mice (Fig. 9). Images of the wound region were taken on days 1, 3, 5 and 9 (Fig. 9a). The extent of wound healing was calculated by comparing the wound size at different timepoint with their initial size at day 1 (Fig. 9b). The wound size was slightly reduced at day 3 in SWFD group, while no difference in control groups, including Bandage or Blank. The significant wound healing could be observed in SWFD group at day 5, and also the average wound healing rates of SWFD group was markedly higher than others controls. Notably, at day 9, the average wound healing rates of SFWD-silver was almost 82%, however 53% in Blank-group and Bandage-group only reached about, and 65% in SFWD. Wound healing is a multistep process, including recruitment of neighbor cells and formation of new tissues. Histological results showed that SWFD group exhibited significant fibroblasts proliferation and granulation tissue formation on day 5, which hardly could be detected in control groups (Figs. 10a–10d). On day 9 (Figs. 10e–10h), fibroblast and granulation tissue occupied the dominant position in SWFD group, and the wound was almost covered with new tissue. These results might suggest that SFWD could promote the wound healing by recruiting more cells and increasing tissue formation on the wound edges.

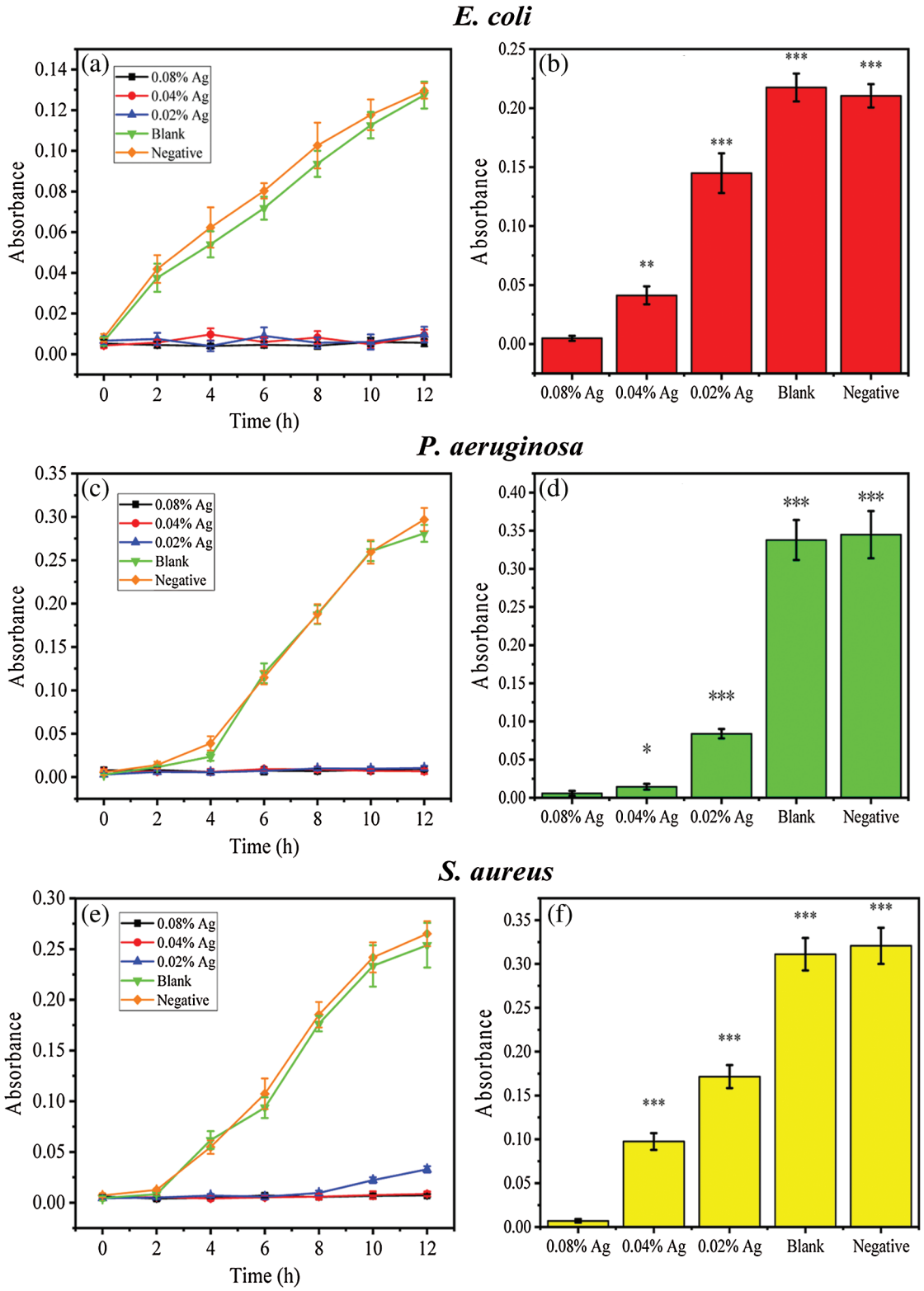

Figure 7: (continued)

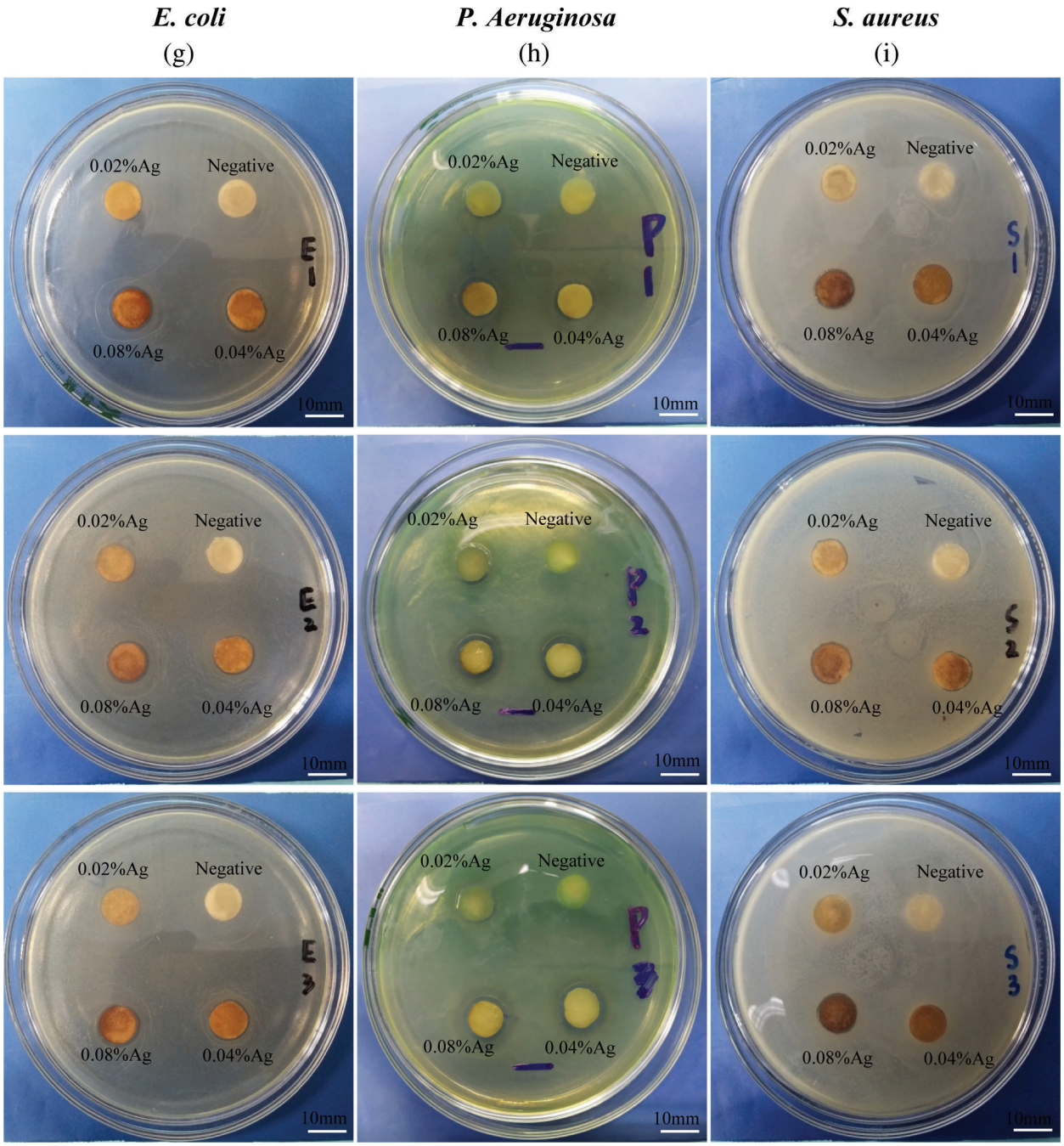

Figure 7: Effect of the Ag-NPs-loaded SFWD on bacterial growth. (a) Growth curve of *Escherichia coli* in 12 h; (b) Ultimate bacterial concentration of *Escherichia coli* at 24 h; (c) Growth curve of *Pseudomonas aeruginosa* in 12 h; (d) Ultimate bacterial concentration of *Pseudomonas aeruginosa* at 24 h; (e) Growth curve of *Staphylococcus aureus* in 12 h; (f) Ultimate bacterial concentration of *Staphylococcus aureus* at 24 h. (g) Inhibition zones in *Escherichia coli* plate with 3 independent tests. (h) Inhibition zones in *Pseudomonas aeruginosa* plate with 3 independent tests. (i) Inhibition zones in *Staphylococcus aureus*plate with 3 independent tests. (*: $p < 0.05$, **: $p < 0.01$, ***: $p < 0.001$, n = 4)

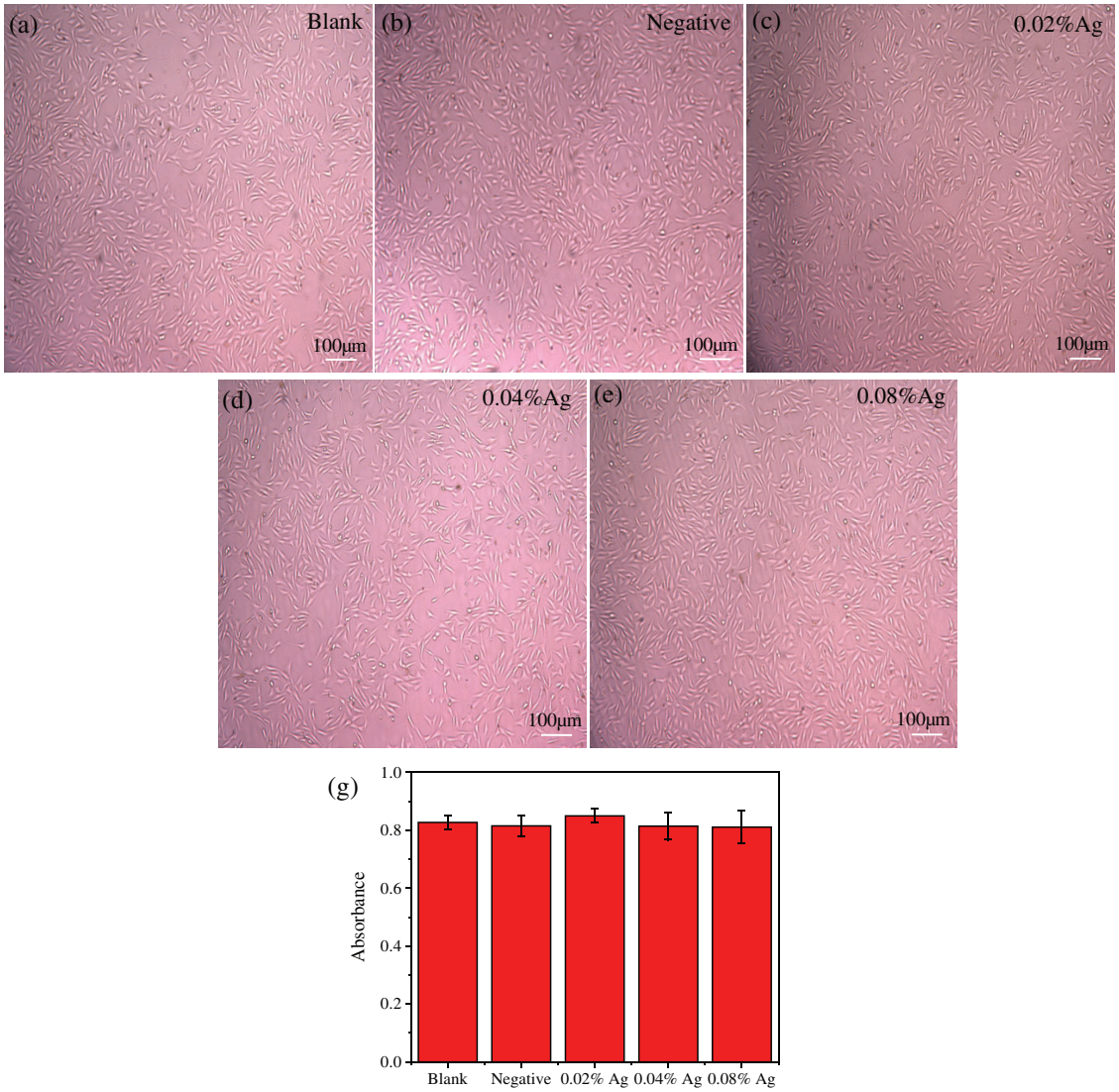

Figure 8: Exhibition of the amount of living cells in experimental and control group. (a–e) the images of each group under microscope; (f) The detection of cell viability was performed by CCK-8. (n = 8)

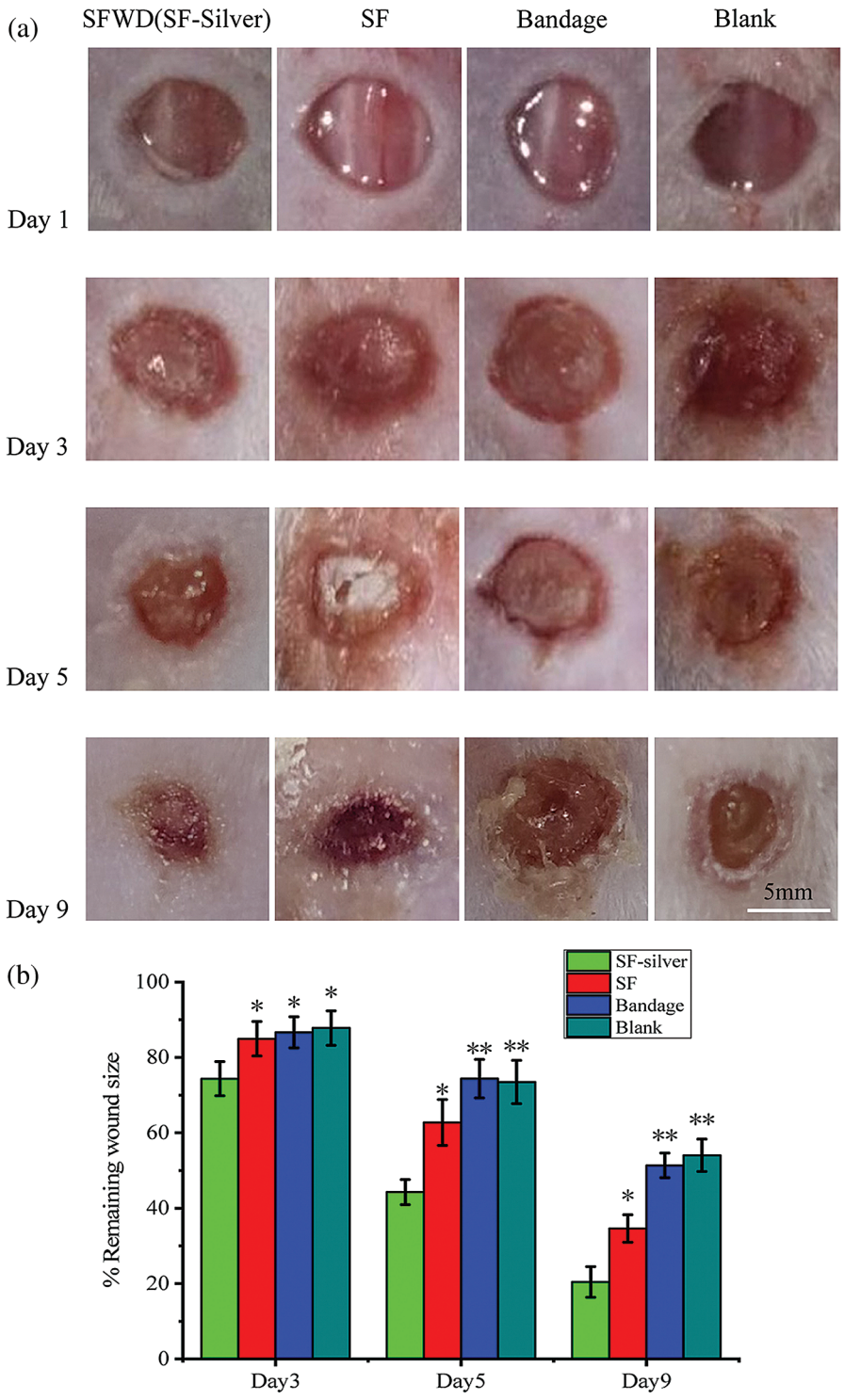

Figure 9: Display of wound healing progress in mice. Day 1 represented the first day of wound management, demonstrating that the mice back wound model was successfully established. (a) Changes of the appearance of back wounds in mice of each group over time; (b) percentage of remaining wound area to original area. SFWD-silver is experiment group with the treatment by SFWD-silver (silver-loaded SFWD); SFWD is experiment group with the treatment by SFWD; Bandage is negative control group; Blank is blank control (*: $p < 0.05$; **: $p < 0.01$; n = 4)

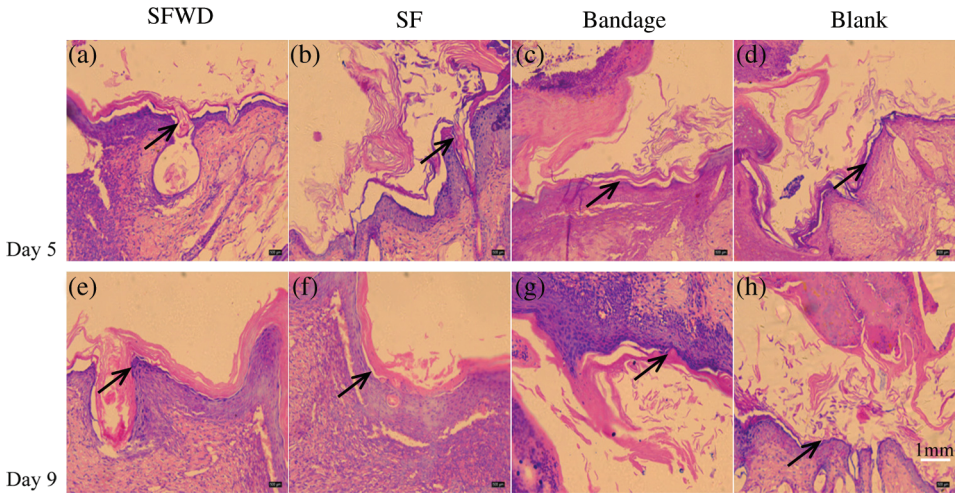

Figure 10: Wound tissue histology. The histology sections of wound tissue at days 5 and 9 after wounding. (a–d): 5 d after wounding; (e–h): 9 d after wounding. The arrow refers to the adsorbed new cells and tissue

4 Conclusions

In this study, we proposed a promising wound dressing from regenerated silk fibroin sponge with sustained release of Ag-NPs. Ag-NPs were fabricated *in situ* by UV irradiation, and silk fibroin served as stabilizer, dispersant and protector. Sponge fabrication and Ag-NPs formation were combined at the same time with low-cost and high efficiency. The Ag-NPs loaded SFWD showed excellent mechanical properties for wound dressing, which could be tuned via altering the parameters of fabrication to match different types of wounds. Ag-NPs loaded SFWD could effectively inhibit the growth of *Escherichia coli*, *Pseudomonas aeruginosa* and *Staphylococcus aureus*. With the increase of silver nitrate (0.02% wt/v, 0.04% wt/v, 0.08% wt/v), it represented more obvious inhibition properties. With exceptional cyto-compatibility, Ag-NPs loaded SFWD presented superior wound healing ability in mouse model, which indicated that Ag-NPs loaded SFWD could be a potential candidate for wound dressing in clinical treatment.

Funding Statement: This research is supported by Chongqing Research Program of Basic Research and Frontier Technology (No. cstc2019jcyj-msxmX0164 to Jiang) and Science and Technology Research Program of Chongqing Municipal Education Commission (No. KJQN201900414 to Jiang) and Special Project on Philosophy and Social Sciences of Chongqing Medical University (No. 201704 to Xiong).

Conflicts of Interest: The authors declare that they have no conflicts of interest to report regarding the present study.

References

1. Li, S., Li, L., Guo, C., Qin, H., Yu, X. (2017). A promising wound dressing material with excellent cytocompatibility and proangiogenesis action for wound healing: Strontium loaded Silk fibroin/Sodium alginate (SF/SA) blend films. *International Journal of Biological Macromolecules, 104,* 969–978. DOI 10.1016/j.ijbiomac.2017.07.020.
2. Pritchard, E. M., Valentin, T., Panilaitis, B., Omenetto, F., Kaplan, D. L. (2013). Antibiotic-Releasing silk biomaterials for infection prevention and treatment. *Advanced Functional Materials, 23(7),* 854–861. DOI 10.1002/adfm.201201636.
3. Han, H., Ning, H., Liu, S., Lu, Q., Fan, Z. et al. (2016). Silk biomaterials with vascularization capacity. *Advanced Functional Materials, 26(3),* 421–432. DOI 10.1002/adfm.201504160.

4. Belanger, K., Dinis, T. M., Taourirt, S., Vidal, G., Kaplan, D. L. et al. (2016). Recent strategies in tissue engineering for guided peripheral nerve regeneration. *Macromolecular Bioscience, 16(4),* 472–481. DOI 10.1002/mabi.201500367.
5. Karahaliloglu, Z., Kilicay, E., Denkbas, E. B. (2017). Antibacterial chitosan/silk sericin 3D porous scaffolds as a wound dressing material. *Artificial Cells, Nanomedicine, and Biotechnology, 45(6),* 1–14. DOI 10.1080/21691401.2016.1203796.
6. Uttayarat, P., Jetawattana, S., Suwanmala, P., Eamsiri, J., Tangthong, T. et al. (2012). Antimicrobial electrospun silk fibroin mats with silver nanoparticles for wound dressing application. *Fibers and Polymers, 13(8),* 999–1006. DOI 10.1007/s12221-012-0999-6.
7. Raia, N. R., Partlow, B. P., McGill, M., Kimmerling, E. P., Ghezzi, C. E. et al. (2017). Enzymatically crosslinked silk-hyaluronic acid hydrogels. *Biomaterials, 131,* 58–67. DOI 10.1016/j.biomaterials.2017.03.046.
8. Wang, X., Cheng, F., Gao, J., Wang, L. (2014). Antibacterial wound dressing from chitosan/polyethylene oxide nanofibers mats embedded with silver nanoparticles. *Journal of Biomaterials Applications, 29(8),* 1086–1095. DOI 10.1177/0885328214554665.
9. Jeannine, C., Jamie, H., Alexander, D. Z., Jennifer, P., Naohiko, I. et al. (2017). Implantable chemotherapy-loaded silk protein materials for neuroblastoma treatment. *International Journal of Cancer, 140(3),* 726–735. DOI 10.1002/ijc.30479.
10. Guang, S., An, Y., Ke, F., Zhao, D., Shen, Y. et al. (2015). Chitosan/silk fibroin composite scaffolds for wound dressing. *Journal of Applied Polymer Science, 132(35),* 1–7. DOI 10.1002/app.42503.
11. Abbott, R. D., Kimmerling, E. P., Cairns, D. M., Kaplan, D. L. (2016). Silk as a biomaterial to support long-term three-dimensional tissue cultures. *ACS Applied Materials & Interfaces, 8(34),* 21861–21868. DOI 10.1021/acsami.5b12114.
12. Dadwal, U., Falank, C., Fairfield, H., Linehan, S., Rosen, C. J. et al. (2016). Tissue-engineered 3D cancer-in-bone modeling: Silk and PUR protocols. *BoneKEy Reports, 5,* 1–8. DOI 10.1038/bonekey.2016.75.
13. Zhang, W., Wray, L. S., Rnjak-Kovacina, J., Xu, L., Zou, D. et al. (2015). Vascularization of hollow channel-modified porous silk scaffolds with endothelial cells for tissue regeneration. *Biomaterials, 56,* 68–77. DOI 10.1016/j.biomaterials.2015.03.053.
14. Tozzi, L., Laurent, P., Di Buduo, C. A., Mu, X., Massaro, A. et al. (2018). Multi-channel silk sponge mimicking bone marrow vascular niche for platelet production. *Biomaterials, 178,* 122–133. DOI 10.1016/j.biomaterials.2018.06.018.
15. Çalamak, S., Erdoğdu, C., Özalp, M., Ulubayram, K. (2014). Silk fibroin based antibacterial bionanotextiles as wound dressing materials. *Materials Science and Engineering: C, 43,* 11–20.
16. Tseng, P., Napier, B., Zhao, S., Mitropoulos, A. N., Applegate, M. B. et al. (2017). Directed assembly of bio-inspired hierarchical materials with controlled nanofibrillar architectures. *Nature Nanotechnology, 12(5),* 474–480. DOI 10.1038/nnano.2017.4.
17. Cai, Z., Mo, X., Zhang, K., Fan, L., Yin, A. et al. (2010). Fabrication of chitosan/silk fibroin composite nanofibers for wound-dressing applications. *International Journal of Molecular Sciences, 11(9),* 3529–3539. DOI 10.3390/ijms11093529.
18. Plowright, R., Dinjaski, N., Zhou, S., Belton, D. J., Kaplan, D. L. et al. (2016). Influence of silk-silica fusion protein design on silica condensation *in vitro* and cellular calcification. *RSC Advances, 6(26),* 21776–21788. DOI 10.1039/C6RA03706B.
19. Rockwood, D. N., Preda, R. C., Yücel, T., Wang, X., Lovett, M. L. et al. (2011). Materials fabrication from Bombyx mori silk fibroin. *Nature Protocols, 6(10),* 1612–1631. DOI 10.1038/nprot.2011.379.
20. Abdelgawad, A. M., Hudson, S. M., Rojas, O. J. (2014). Antimicrobial wound dressing nanofiber mats from multicomponent (chitosan/silver-NPs/polyvinyl alcohol) systems. *Carbohydrate Polymers, 100,* 166–178. DOI 10.1016/j.carbpol.2012.12.043.
21. Zhao, S., Chen, Y., Partlow, B. P., Golding, A. S., Tseng, P. et al. (2016). Bio-functionalized silk hydrogel microfluidic systems. *Biomaterials, 93,* 60–70. DOI 10.1016/j.biomaterials.2016.03.041.

22. Min, S., Gao, X., Han, C., Chen, Y., Yang, M. et al. (2012). Preparation of a silk fibroin spongy wound dressing and its therapeutic efficiency in skin defects. *Journal of Biomaterials Science-Polymer Edition, 23(1–4),* 97–110. DOI 10.1163/092050610X543609.
23. Park, W. H., Jeong, L., Kim, M. H., Jung, J., Min, B. M. (2014). Effect of silk fibroin nanofibers containing silver sulfadiazine on wound healing. *International Journal of Nanomedicine, 9,* 5277–5287. DOI 10.2147/IJN.S71295.
24. Yang, X., Fan, L., Ma, L., Wang, Y., Lin, S. et al. (2017). Green electrospun Manuka honey/silk fibroin fibrous matrices as potential wound dressing. *Materials & Design, 119,* 76–84. DOI 10.1016/j.matdes.2017.01.023.
25. Gil, E. S., Panilaitis, B., Bellas, E., Kaplan, D. L. (2013). Functionalized silk biomaterials for wound healing. *Advanced Healthcare Materials, 2(1),* 206–217. DOI 10.1002/adhm.201200192.
26. Vasconcelos, A., Gomes, A. C., Cavaco-Paulo, A. (2012). Novel silk fibroin/elastin wound dressings. *Acta Biomaterialia, 8(8),* 3049–3060. DOI 10.1016/j.actbio.2012.04.035.
27. Frazier, T. P., Bowles, A., Lee, S., Abbott, R., Tucker., H. A. et al. (2016). Serially transplanted nonpericytic CD1462 adipose stromal/stem cells in silk bioscaffolds regenerate serially transplanted nonpericytic CD1462 adipose stromal/stem cells in silk bioscaffolds regenerate adipose tissue *In Vivo*. *Stem Cells, 34(4),* 1097–1111. DOI 10.1002/stem.2325.
28. Teuschl, A. H., Zipperle, J., Huber-Gries, C., Kaplan, D. L. (2017). Silk fibroin based carrier system for delivery of fibrinogen and thrombin as coagulant supplements. *Journal of Biomedical Materials Research Part A, 105(3),* 687–696. DOI 10.1002/jbm.a.35940.
29. Yang, L., Zheng, Z., Qian, C., Wu, J., Liu, Y. et al. (2017). Curcumin-functionalized silk biomaterials for anti-aging utility. *Journal of Colloid and Interface Science, 496,* 66–77. DOI 10.1016/j.jcis.2017.01.115.
30. Stoppel, W. L., Gao, A. E., Greaney, A. M., Partlow, B. P., Bretherton, R. C. et al. (2016). Elastic, silk-cardiac extracellular matrix hydrogels exhibit time-dependent stiffening that modulates cardiac fibroblast response. *Journal of Biomedical Materials Research Part A, 104(12),* 3058–3072. DOI 10.1002/jbm.a.35850.
31. Zhang, Q., Yan, S., You, R., Kaplan, D. L., Liu, Y. et al. (2016). Multichannel silk protein/laminin grafts for spinal cord injury repair. *Journal of Biomedical Materials Research Part A, 104(12),* 3045–3057. DOI 10.1002/jbm.a.35851.
32. Farokhi, M., Mottaghitalab, F., Fatahi, Y., Khademhosseini, A., Kaplan, D. L. (2018). Overview of silk fibroin use in wound dressings. *Trends in Biotechnology, 36(9),* 907–922. DOI 10.1016/j.tibtech.2018.04.004.
33. Calamak, S., Aksoy, E. A., Ertas, N., Erdogdu, C., Sagıroglu, M. et al. (2015). Ag/silk fibroin nanofibers: Effect of fibroin morphology on Ag^{+} release and antibacterial activity. *European Polymer Journal, 67,* 99–112. DOI 10.1016/j.eurpolymj.2015.03.068.
34. Belanger, K., Dinis, T. M., Taourirt, S., Vidal, G., Kaplan, D. L. et al. (2016). Recent strategies in tissue engineering for guided peripheral nerve regeneration. *Macromolecular Bioscience, 16(4),* 472–481. DOI 10.1002/mabi.201500367.
35. Thurber, A. E., Omenetto, F. G., Kaplan, D. L. (2015). *In vivo* bioresponses to silk proteins. *Biomaterials, 71,* 145–157. DOI 10.1016/j.biomaterials.2015.08.039.
36. Bradner, S. A., Partlow, B. P., Cebe, P., Omenetto, F. G., Kaplan, D. L. (2017). Fabrication of elastomeric silk fibers. *Biopolymers, 107(9),* e23030. DOI 10.1002/bip.23030.